Activation of Soluble Guanylyl Cyclase by Four-Coordinate Metalloporphyrins: Evidence for a Role for Porphyrin Conformation†

Heather S. Carr,‡ Dat Tran,§ Mark F. Reynolds,‡ Judith N. Burstyn,*,‡ and Thomas G. Spiro*,§

Department of Chemistry, University of Wisconsin−Madison, 1101 University Avenue, Madison, Wisconsin 53706, and Hoyt Laboratory, Princeton University, Washington Road, Princeton, New Jersey 08544

Received April 17, 2001; Revised Manuscript Received June 22, 2001

ABSTRACT: Four-coordinate metalloporphyrins activate soluble guanylyl cyclase. Ni^{II}PPIX and Cu^{II}PPIX are high affinity activators, with activation constants of 24 and 17 nM, respectively. Both metalloporphyrins remain stably bound to the enzyme, enabling spectroscopic characterization of the Ni(II)- and Cu(II)-reconstituted protein. Electronic absorption and resonance Raman spectroscopy reveal that Ni^{II}PPIX remains four coordinate when bound to soluble guanylyl cyclase. Analysis of the vibrational frequencies of the Ni(II)-reconstituted enzyme suggests that the protein imposes a constraining force on the porphyrin, favoring a planar conformation. Spectroscopic data for the Cu(II)-substituted protein are also consistent with four coordination. The intensification of the vibrational modes of the peripheral vinyl groups in both Ni(II)- and Cu(II)-reconstituted soluble guanylyl cyclase are consistent with a substantial influence of the protein on the porphyrin environment. Together these data support a model where activation of soluble guanylyl cyclase correlates with the absence of a metal-to-proximal histidine bond and with decreased conformational freedom for the tetrapyrrole in the activated state.

Nitric oxide (NO) is an important physiological signaling molecule, and a complete understanding of how NO regulates it primary target, soluble guanylyl cyclase, has yet to be achieved. Soluble guanylyl cyclase (sGC)[1] is a heterodimeric heme protein that catalyzes the transformation of GTP to cGMP, a key intracellular second messenger (*1*). Although the *b*-type heme (Fe^{II}PPIX) is not required for sGC to exhibit basal catalytic activity, it is essential for NO-induced activation (*2*). The sGC heme in its resting state is either 5- or 6-coordinate, with histidine(s) as the axial ligand (*3*−*6*). NO coordinates to the heme cofactor, breaking the iron−histidine bond(s) to form a five-coordinate species (*3, 6, 7*). It is proposed that the scission of the metal−histidine bond mediates a conformational change that leads to the activation of the enzyme (*8*); however, the details of this process are unknown.

Tetrapyrroles other than NO−heme *b* influence the activity of sGC. The free base of heme *b*, protoporphyrin IX (PPIX), activates sGC, as do mesoporphyrin and hematoporphyrin (*9, 10*). All of these tetrapyrroles have propionate substituents at the 6 and 7 positions, while the substituents at the 2 and 4 positions are vinyl and ethyl or hydroxyethyl, respectively. Other alterations of the propionate or vinyl substituents render the tetrapyrroles inhibitory or ineffective as activators (*9*). Metalloporphyrins other than heme *b* also affect sGC. ZnPPIX, CoPPIX, and MnPPIX all inhibit basal sGC activity (*8, 9, 11*). Only CoPPIX and FePPIX activate sGC in the presence of NO, an observation that has been correlated with the formation of a five-coordinate nitrosyl adduct (*8*). Kinetic analysis reveals that PPIX and NO−heme activate sGC by similar mechanisms, implying that other porphyrins may influence the protein in the same manner (*2*). Activation of sGC by non-native porphyrins and metalloporphyrins may therefore provide insight into the manner in which the activated conformation is stabilized.

As part of our ongoing studies of the mechanism of activation of sGC, we have investigated the effects of four-coordinate metalloporphyrins on the activity of sGC. The data described above suggest that the presence of the heme *b* periphery and the absence of a metal histidine bond are necessary for activation of sGC. To test this hypothesis, the effects of air-stable Ni^{II}PPIX and Cu^{II}PPIX, electron-rich porphyrins that should remain four-coordinate, were studied by kinetic and spectroscopic techniques. As described herein, both metalloporphyrins are activators and they are 4-coordinate when bound to sGC. The data presented suggest that not only is the peripheral substitution pattern important in sGC activation, but the conformation of the tetrapyrrole is also of consequence.

EXPERIMENTAL METHODS

Materials. Bovine lung was obtained from Schroedl's Meat Market in Jefferson, WI. The anti-BSA−agarose resin was

† This work was supported in part by NIH Grants GM-33576 (T.G.S.) and HL-65217 (J.N.B). NIH fellowship support is gratefully acknowledged (GM-18949, D.T.; GM-08505, H.S.C.; GM-08293, M.F.R.).

* To whom correspondence should be addressed. J.N.B.: phone (608) 262-0328; fax (608) 262-6143; E-mail burstyn@chem.wisc.edu. T.G.S.: phone (609) 258-3907; fax (609) 258-0348; E-mail spiro@chemvax.princeton.edu.

‡ University of Wisconsin−Madison.

§ Princeton University.

[1] Abbreviations: sGC, soluble guanylyl cyclase; PPIX, protoporphyrin IX; TEA, triethanolamine; DTT, D,L-dithiothreitol; SNAP, *S*-nitroso-*N*-acetyl penicillamine; IBMX, isobutylmethylxanthine; DMF, dimethyl formamide; DMSO, dimethyl sulfoxide; μBCA, micro bicinchoninic acid protein assay; RR, resonance Raman; pip, piperidine; CTAB, cetyl trimethylammonium bromide; cyt *c*; cytochrome *c*; MesoP, mesoporphyrin; MP-11, microperoxidase 11, an 11-amino acid heme bearing peptide derived from cyt *c*; P, porphine; MES, 2-(*N*-morpholino)ethanesulfonic acid; P_i, phosphate buffer.

10.1021/bi010777k CCC: $22.00
Published on Web 07/12/2002

prepared using an AminoLink kit from Pierce (Rockford, IL) and anti-BSA antibodies from Sigma. [α-^{32}P]GTP was obtained from NEN-DuPont. Orange-A resin was obtained from Amicon-Millipore (Bedford, MA). PPIX, Cu^{II}PPIX, and Ni^{II}PPIX were purchased from Porphyrin Products (Logan, UT) or MidCentury Chemical (Posen, IL). SNAP was a gift from Dr. Jon Fukuto, UCLA School of Medicine. All other reagents were obtained from standard sources.

Methods. Purification of Soluble Guanylyl Cyclase. Protein was purified as described (*12*). In sequence the procedure involves ion exchange, dye-ligand, size-exclusion, and antibody affinity chromatographies. The enzyme had a specific activity of 28.3 ± 0.4 nmol of cGMP min^{-1} (mg of protein)$^{-1}$ and was activated 27-fold by SNAP. Enzyme used for spectroscopic experiments was purified by the same method with an additional step. The AcA34 size-exclusion resin was equilibrated in 25 mM TEA, pH 7.4, 5 mM DTT, 0.2 mM benzamidine, 0.5 mg/L trypsin inhibitor, and leupeptin buffer that was 20 mM in $MgCl_2$. Protein was eluted in the same buffer and adsorbed onto 100 mL of Orange A resin for 60 min. The resin was packed in a 2.4 cm diameter Pharmacia column, and sGC was eluted with a linear gradient of TEA-DTT buffer from 0 to 1 M KCl at a flow rate of 1.8 mL/min. The fractions were assayed, collected, concentrated, and passed over an anti-BSA agarose column before further concentration and storage. sGC isolated by this procedure had a specific activity of 14.1 ± 0.6 nmol of cGMP min^{-1} mg^{-1} and was activated 110-fold by SNAP. Both procedures produced sGC that was BSA-free by Western blot analysis.

Soluble Guanylyl Cyclase Activity Assay. The activity of sGC was determined as previously reported (*13*). Unless otherwise noted, each enzyme reaction was conducted in a total volume of 200 μL containing 40 mM TEA pH 7.4, 10 mM DTT, 1 mM GTP, 3 mM $MgCl_2$, 0.3 mM IBMX, 2.5 pmol [α-^{32}P]GTP, and variable amounts of sGC. The reaction was carried out for 10 min at 37 °C and stopped by adding 10 μL of 0.5 M EDTA. [^{32}P]cGMP was separated from [α -^{32}P]GTP by TLC on PEI-F cellulose plates in 0.15 M LiCl. [^{32}P]cGMP was eluted into 10 mL of Biosafe II scintillation cocktail and quantitated in a Beckman LS-6000 scintillation counter. SNAP (100 μM) was used as the NO donor. Protein concentrations were determined by the μBCA assay using γ-globulin as the standard. Samples containing DTT were read against a standard curve containing DTT, or the DTT was removed by spin dialysis in Microcon concentrators. All data were obtained by taking the average value of at least three separate determinations and are expressed as the mean plus or minus the standard deviation. Some experiments were conducted in the presence of variable concentrations of synthetic porphyrins, in which case the experimental details are found in the figure or table legends. K_{act} (apparent binding constant for the activator) and V_{max} values were calculated by nonlinear least-squares fits of the initial velocities to the Michaelis−Menten equation using the program HyperO (*14*).

Porphyrin Solution Preparation. Stock solutions of PPIX, Cu^{II}PPIX, and Ni^{II}PPIX were prepared freshly for each experiment by dissolving the porphyrin in DMSO followed by dilution into 25 mM TEA, pH 7.4. The concentration of DMSO in the assay never exceeded 0.5% (*11*). All other stock solutions were prepared in deionized H_2O or 25 mM TEA, pH 7.4.

Heme Depletion and Reconstitution. Heme was removed by a modification of a previously described method (*15*). Protein was incubated at 37 °C for 10 min in the presence of 0.5% Tween-20. The protein solution was then adsorbed for 10 min onto one volume of Q-Sepharose Fast Flow (Pharmacia) resin that had been equilibrated with 25 mM TEA, pH 7.8, and 50 mM NaCl. The resin was packed in a Pierce minicolumn and washed with three column volumes of TEA, pH 7.8, followed by elution with two column volumes of 25 mM TEA, pH 7.4, and 0.7 M NaCl. The sGC was then incubated for 10 min on ice with a 2-fold molar excess of the desired porphyrin, followed by spin-dialysis to remove unbound porphyrin. Reconstituted samples were assayed for activity prior to acquisition of optical spectra. Electronic absorption spectra were recorded on a Cary-4 Bio UV−visible spectrophotometer. The Ni and Cu content of the reconstituted protein was determined by graphite furnace atomic absorption spectrometry on a Perkin-Elmer model 3030 with a HGA-300 furnace controller or by analysis at the University of Wisconsin Soil and Plant Analysis Lab.

Resonance Raman Spectroscopy. Raman spectra were obtained with a Spex 1877 triple monochromator equipped with a water-cooled intensified photodiode array detector, as described previously (*16*). Data were collected in a backscattering geometry from samples in spinning NMR tubes. The excitation source for Cu^{II}PPIX and Ni^{II}PPIX (∼1 mM in 5% DMSO/CCl_4) was a Coherent Innova 100-K3A Kr^+ laser (406 or 413 nm). Ni^{II}sGC and Cu^{II}sGC protein solutions were excited at ∼395 nm with the second harmonic of a Ti:sapphire laser (TU-UV), which was pumped by the second harmonic (20 W) of a 1 kHz Q-switched Nd:YLF laser (Photonics International GM-30-527) (*17*). The laser power at the sample was ∼20 mW, and the spectral bandwidth was 3 cm^{-1}. Raman shifts were calibrated with known solvent spectra (CCl_4 or DMF), and Grams/32 software (version 5, Galactic) was used for spectral analysis.

RESULTS

Activity Measurements. Both Ni^{II}PPIX, and Cu^{II}PPIX are high-affinity activators of sGC. When sGC was depleted of endogenous heme and reconstituted with Ni^{II}PPIX and Cu^{II}-PPIX, the enzyme was significantly activated by both metalloporphyrins (Figure 1). The extent of activation differed depending on the central metal ion; Ni^{II}sGC was activated 63-fold and Cu^{II}sGC 32-fold over the basal catalytic activity. The Michaelis−Menten parameters were determined for activation of sGC by Ni^{II}PPIX and Cu^{II}PPIX (Figure 2). The two activators differed in the maximal velocity attained, but both exhibited high affinity for the enzyme (Table 1). Consistent with the results obtained in reconstitution experiments, Ni^{II}sGC achieved a higher maximal velocity than Cu^{II}sGC, demonstrating that Ni^{II}PPIX was a more effective activator. The activation constants (K_{act}) for the two metalloporphyrins were very similar to one another, 24 and 17 nM for Ni^{II}PPIX and Cu^{II}PPIX, respectively, and both were nearly identical to the activation constant for PPIX obtained with the same enzyme preparation (22 nM). PPIX is known to be a high-affinity activator of sGC, and the activation constants previously determined of 8 nM (*9*) and 11 nM (*11*) are of the same magnitude.

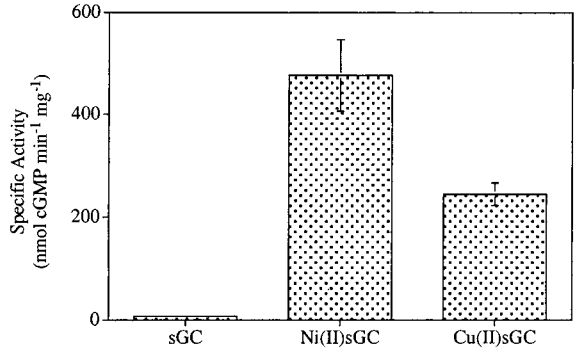

FIGURE 1: Activation of sGC by Ni^{II}PPIX and Cu^{II}PPIX. The enzyme was heme-depleted, reconstituted with porphyrin, and assayed for cGMP formation. The enzyme concentration in the assay was 150 nM. Each data point was measured in triplicate. (Data shown are from one experiment and are representative of multiple experiments, although the absolute value of specific activity varies between preparations.) The error bars represent the deviation from the mean value.

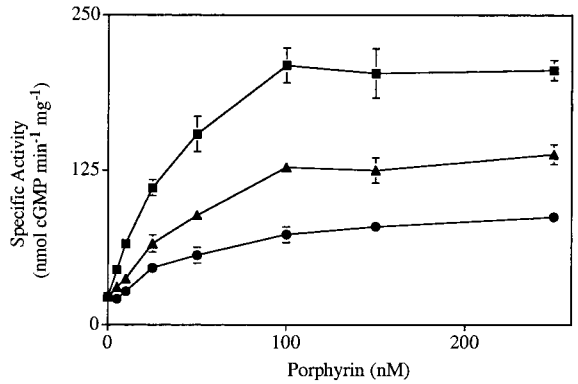

FIGURE 2: Concentration dependence of activation of sGC by non-native porphyrins. Enzyme was assayed in the presence of PPIX (squares), Ni^{II}PPIX (triangles), and Cu^{II}PPIX (circles) varying in concentration from 0 to 250 nM. The enzyme concentration in the assay was 89−94 nM. Each sample was assayed in triplicate in two separate experiments. Error bars show the deviation from the mean, and where error bars do not appear, the error is smaller than the plotted point.

Table 1: Michaelis−Menten Parameters for Activation of sGC by Non-Native Porphyrins[a]

sample	K_{act} (nM)	V_{max} (nmol min^{-1} mg^{-1})
PPIX	21.8 ± 1.8	209 ± 8
Ni^{II}PPIX	23.7 ± 2.1	150 ± 5
Cu^{II}PPIX	17.0 ± 1.6	84 ± 4

[a] K_{act} and V_{max} were determined by nonlinear fit using the program *HyperO*. The conditions were as described in Figure 2.

It has been suggested that two requirements for porphyrin-induced activation of sGC are the absence of a metal−axial histidine bond and the presence of the protoporphyrin IX peripheral substitution pattern (*8*). The data obtained demonstrating that both Ni^{II}PPIX and Cu^{II}PPIX were high-affinity activators suggested that both metalloporphyrins remained 4-coordinate in the enzyme. To determine whether Ni^{II}sGC and Cu^{II}sGC were suitable for spectroscopic analysis, the stability of the two reconstituted proteins was determined. Ni^{II}PPIX and Cu^{II}PPIX form adducts with sGC that are stable over long periods of time; Ni^{II}sGC and Cu^{II}sGC retained high catalytic activity for at least 1 h at 37 °C. In contrast, PPIX does not form a stable complex with sGC and the high activity is lost within 20 min (*9, 11*). Reconstitution of sGC with PPIX, under conditions identical to those employed for Ni^{II}PPIX and Cu^{II}PPIX, does not result in porphyrin-replete enzyme, and spectroscopic characterization of the PPIX-reconstituted protein is therefore not possible. The high stability of Ni^{II}sGC and Cu^{II}sGC rendered them well suited for spectroscopic characterization.

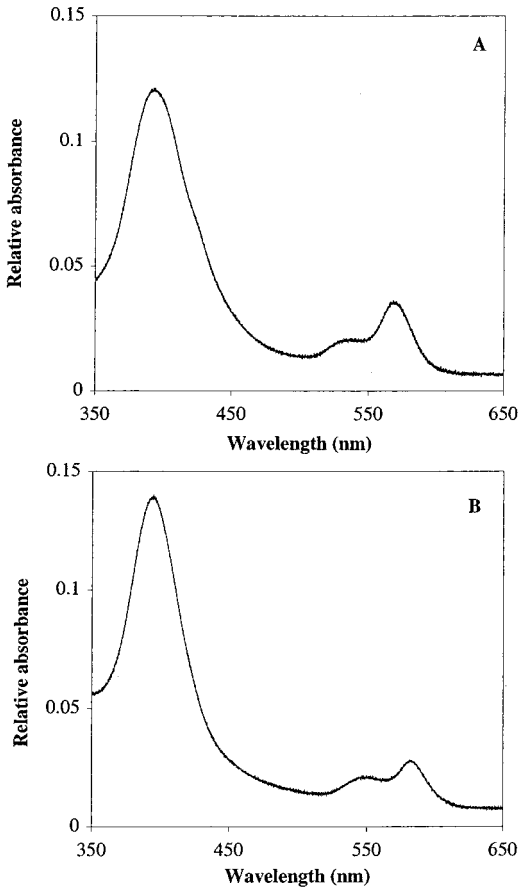

FIGURE 3: Electronic spectra of (A) Ni^{II}sGC (4 μM) and (B) Cu^{II}-sGC (4 μM) in 25 mM TEA buffer, pH 7.4, and 50 mM NaCl. Absorption maxima are the following: (A) Soret, 390 nm, β, 533 nm, and α, 564 nm; (B) Soret, 393 nm, β, 541 nm, and α, 577 nm. These data are also reported in Tables 2 and 3, respectively.

Electronic Absorption Spectra. Ni^{II}sGC and Cu^{II}sGC were characterized by electronic absorption spectroscopy. In the absence of a detergent in aqueous solution, both Ni^{II}PPIX and Cu^{II}PPIX are highly aggregated, as evidenced by broad and shallow Soret absorptions. In contrast, Ni^{II}sGC and Cu^{II}-sGC give sharp, well-defined spectra in aqueous buffered solution (Figure 3). Both show significantly blue-shifted Soret bands in comparison to the free porphyrin in noncoordinating solvents (Tables 2 and 3). The Soret absorption for Ni^{II}sGC appears at 390 nm, while that of Ni^{II}PPIX in DMSO appears at 401 nm. The Soret absorption for Cu^{II}-sGC appears at 393 nm, significantly shifted from the free porphyrin, which absorbs at 407 nm. The α and β bands of the Ni(II)- and Cu(II)-substituted sGC are slightly red-shifted, appearing at 564 and 533 nm for Ni^{II}sGC and at 577 and 541 nm for Cu^{II}sGC, respectively (Tables 2 and 3). The ϵ_{390} for Ni^{II}sGC is calculated to be 93 300 ± 9300 M^{-1} cm^{-1}, and ϵ_{393} is approximately 56 400 ± 3500 M^{-1} cm^{-1} for Cu^{II}-sGC. Both of these values are considerably lower than the Soret extinction coefficients in DMSO (ϵ_{401} = 110 700 M^{-1}

Table 2: Comparison of the Electronic Absorption Maxima of Ni^{II}sGC with Those of Other Ni(II)-Reconstituted Proteins and Model Systems

sample	Soret (nm)	β (nm)	α (nm)	coord no.	ref
Ni^{II}Hb in P_i buffer	397	558		4	18
Ni^{II}Hb in P_i buffer	419		580	5	18
Ni^{II}Mb in P_i buffer	418	540	583	5	18
Ni^{II}PPIX in CTAB/base	400	522	560	4	18
Ni^{II}PPIX in pyridine	431		588	6	18
Ni^{II}PPIX in TEA	395 (broad)	543	571	4	this work
Ni^{II}PPIX in TEA/Tween-20	401	525	561	4	this work
Ni^{II}PPIX in DMSO	401	524	561	4	this work
Ni^{II}sGC in TEA	390	533	564	4	this work

Table 3: Comparison of the Electronic Absorption Maxima of Cu^{II}sGC with Those of Other Cu(II)-Reconstituted Proteins and Model Complexes

sample	Soret (nm)	β (nm)	α (nm)	coord no.	ref
Cu^{II}Hb in P_i buffer	405	536	569	4	36
Cu^{II}Hb in P_i buffer	418			5	36
Cu^{II}Mb in P_i buffer	425	545	585	5	35, 36
Cu^{II}PPIX in MES buffer	385	540	577	4	35
Cu^{II}PPIX in TEA buffer	389	550	582	4	this work
Cu^{II}PPIX in TEA/Tween-20	407	533	571	4	this work
Cu^{II}PPIX in DMSO	407	534	572	4	this work
Cu^{II}sGC in TEA	393	541	577	4	this work

cm^{-1} for Ni^{II}PPIX, $\epsilon_{407} = 141\,300\ M^{-1}\ cm^{-1}$) but higher than the porphyrins in aqueous solution ($\epsilon_{395} = 28\,900\ M^{-1}\ cm^{-1}$ for Ni^{II}PPIX, $\epsilon_{389} = 45\,000\ M^{-1}\ cm^{-1}$ for Cu^{II}PPIX in 25 mM TEA pH 7.4).

Comparison of the electronic absorption maxima of Ni^{II}sGC and Cu^{II}sGC with those of other Ni^{II}PPIX- and Cu^{II}PPIX-reconstituted proteins and model complexes suggests that both porphyrins remain 4-coordinate when bound to sGC. Both Ni^{II}sGC and Cu^{II}sGC exhibit substantially higher energy Soret absorption maxima than is typically observed for the metalloporphyrins in other environments (Tables 2 and 3). The Soret band is very close to 400 nm for Ni^{II}PPIX in noncoordinating solvents or in the Hb α chains, whereas this band is shifted by approximately 20 nm to longer wavelength in the Hb β chains or in Mb (*18*). The position of the Soret band correlates well with the apparent coordination geometry, with 4-coordinate Ni^{II}PPIX absorbing near 400 nm and 5-coordinate Ni^{II}PPIX absorbing near 420 nm. Addition of a sixth ligand, as occurs when Ni^{II}PPIX is dissolved in pyridine, shifts the Soret absorption an additional 10 nm to 431 nm. Similarly, the Soret absorption of Cu^{II}sGC band is blue-shifted relative to Cu^{II}PPIX in noncoordinating solvents or in the Hb α chains, whereas it is red-shifted in the β chains or in Cu^{II}Mb (*18*, *19*), where coordination by the proximal histidine is expected. The electronic absorption data therefore suggest that both Ni^{II}sGC and Cu^{II}sGC contain 4-coordinate porphyrins where the proximal histidine is not bound. This conclusion is consistent with the high activity observed for these metalloporphyrin-substituted proteins and provides further support for the proposal that loss of the axial ligand is one requirement for enzyme activation.

Resonance Raman Spectra. Resonance Raman spectroscopy provides a more definitive tool to examine the coordination environment of metalloporphyrins and has been employed successfully in the characterization of a variety of metalloporphyrin-substituted heme proteins. The high energy of the Soret absorption maxima in Ni^{II}sGC and Cu^{II}sGC rendered excitation with the 406.7 nm Kr^+ laser line inefficient. Excitation at this wavelength gave good quality spectra for the protein-free chromophores but very weak spectra for the sGC samples. Consequently, excitation at ~395 nm was employed to obtain spectra of the metalloporphyrin-reconstituted proteins. The resonance Raman (RR) spectra of Ni^{II}sGC and Cu^{II}sGC are shown in Figures 4 and 5, and listings of peak positions and assignments are presented in Tables 4 and 5. Because of band overlaps, the frequencies were determined by peak fitting, keeping the bandwidths to less than 25 cm^{-1}, as illustrated for Ni^{II}PPIX in Figure 6. All mode assignments are based on previous data; the RR bands have all been assigned to vibrational modes of the porphyrin ring and the vinyl substituents (*20*). Comparison of selected vibrational modes of Ni^{II}sGC and those of other Ni^{II}PPIX-substituted metalloproteins and models are presented in Table 6. The motions that give rise to the vibrational modes discussed here have been assigned and discussed in detail elsewhere (*20*), and RR data presented here are those which provide information on three distinct features of the metalloporphyrin environment in sGC: the coordination number; the porphyrin planarity; the porphyrin periphery. The interpretation of the RR spectra are presented in detail below.

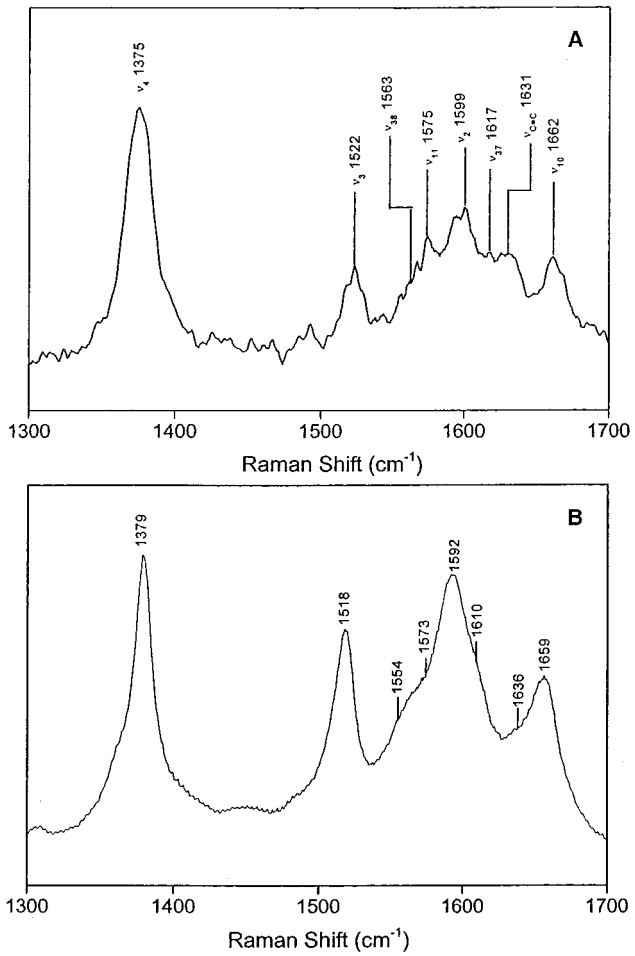

FIGURE 4: Resonance Raman spectrum of Ni^{II}sGC (29 μM) in 25 mM TEA buffer, pH 7.4, and 50 mM NaCl at room temperature (395 nm excitation) (A) and, for comparison, Ni^{II}PPIX in 5% DMSO/CCl_4 (406 nm excitation) (B). Vibrational frequencies are reported in Table 4.

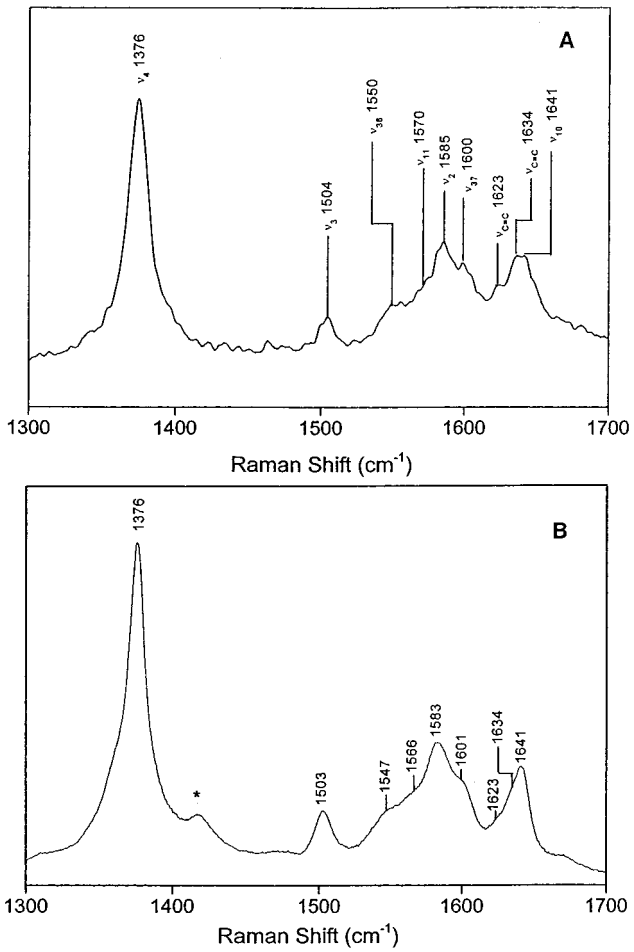

FIGURE 5: Resonance Raman spectrum of Cu^{II}sGC (20 μM) in 25 mM TEA buffer, pH 7.4, and 50 mM NaCl at room temperature (395 nm excitation) (A) and, for comparison, Cu^{II}PPIX in 5% DMSO/CCl_4 (406 nm excitation) (B). The asterisk marks a vibrational mode assigned to DMSO. Vibrational frequencies are reported in Table 5.

Table 4: Raman Frequencies for Ni^{II}PPIX and Ni^{II}sGC in the 1400−1700 cm^{-1} Region Obtained from Spectral Deconvolution and Fitting

vibrational mode	Ni^{II}PPIX frequency (cm^{-1})	Ni^{II}sGC frequency (cm^{-1})
ν_3	1518	1522
ν_{38}	1557	1563
ν_{11}	1575	1575
ν_2	1592	1599
ν_7	1611	1617
$\nu_{c=c}$(vinyl)	1635	1631
ν_{10}	1650, 1658	1662

Coordination Number. RR data are consistent with 4-coordination in both Ni^{II}sGC and Cu^{II}sGC. The porphyrin vibrational frequencies above 1300 cm^{-1} are sensitive to axial coordination of the central metal ion, primarily because of their dependence on the porphyrin core size (*20*). The effect is particularly pronounced for Ni(II), which is converted from low- to high-spin upon binding one or two axial ligands. The in-plane antibonding $d_{x^2-y^2}$ orbital is empty in the 4-coordinate complex but contains an electron in 5- and 6-coordinate complexes, resulting in expansion of the core-size and large downshifts of the porphyrin frequencies (*18, 19, 21*). It is therefore straightforward to determine whether axial ligands are bound. For example in Ni^{II}Mb and the β chains of Ni^{II}Hb, the prominent ν_4 band appears at ~1365 cm^{-1} when the proximal histidine ligand is bound in the protein, while that of the free metalloporphyrin appears at 1378 cm^{-1} (Table 6) (*18, 19*). In the Ni^{II}sGC RR spectrum (Figure 4), there is no shift in ν_4 or any other porphyrin skeletal mode, establishing that the Ni^{II}PPIX remains 4-coordinate when bound to the protein. Ni^{II}sGC appears most similar to the α chains of Ni^{II}Hb, where the proximal histidine is not bound (Table 6). The RR data strongly suggest that in Ni^{II}sGC the axial histidine remains unbound, and this conclusion is also supported by the electronic absorption data described previously.

Table 5: Raman Frequencies for Cu^{II}PPIX, Cu^{II}PPIX(pip), and Cu^{II}sGC in the 1400−1700 cm^{-1} Region Obtained from Spectral Deconvolution and Fitting

vibrational mode	Cu^{II}PPIX freq (cm^{-1})	Cu^{II}PPIX(pip) freq (cm^{-1})	Cu^{II}sGC freq (cm^{-1})
ν_3	1503	1499	1504
ν_{38}	1547	1547	1550
ν_{11}	1566	1562	1570
ν_2	1583	1578	1585
ν_{37}	1601	1598	1600
$\nu_{c=c}$(vinyl)	1623, 1634	1620, 1629	1623, 1634
ν_{10}	1641	1637	1641

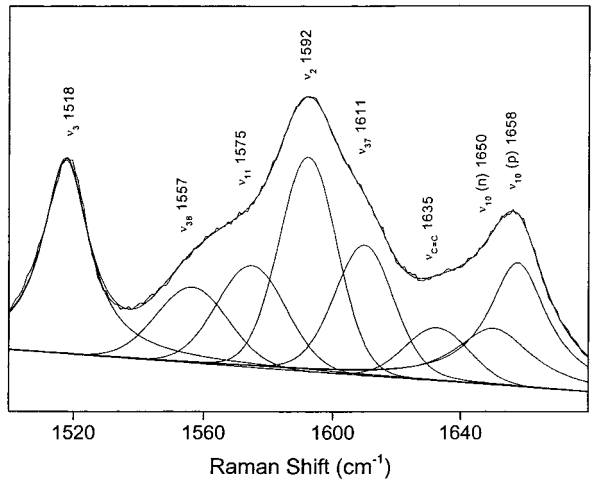

FIGURE 6: Deconvolution of the resonance Raman spectrum of Ni^{II}PPIX. The spectrum was assigned as described in the Results section.

Although less definitive, the RR data for Cu^{II}sGC are also consistent with the absence of the axial histidine ligand. Determination of coordination is less straightforward for Cu(II) than for Ni(II) because no spin-state change is available for the d^9 electronic configuration. Axial ligands bind only weakly to Cu(II), due to the filled d_{z^2} orbital, and the $d_{x^2-y^2}$ orbital is singly occupied in both 4- or 5-coordinate complexes. An axial ligand is, however, expected to expand the porphyrin core slightly via nonbonded contacts among the ligating atoms, and this expansion should be detectable in small shifts in the RR frequencies. Consistent with this expectation, we find 3−4 cm^{-1} downshifts of the core-size marker bands ν_3, ν_{11}, ν_2, ν_{37}, and ν_{10} when Cu^{II}PPIX is dissolved in the coordinating solvent piperidine (Table 5). Corresponding downshifts are not observed for Cu^{II}PPIX in sGC, suggesting that the metalloporphyrin remains 4-coordinate in the protein (Figure 5 and Table 5). Again the RR data are consistent with the electronic absorption data that

Table 6: Comparison of the High-Frequency Vibrational Modes of Ni^{II}sGC and Cu^{II}sGC with Those of Other Ni(II)- and Cu(II)-Substituted Heme Proteins and Model Compounds[a]

			Raman peak frequencies (cm^{-1})				
coord no.	porphyrin	solvent	ν_4	ν_3	ν_2	ν_{10}	ref
4	Ni^{II}sGC	TEA, pH 7.4	1375	1522	1599	1662	this work
	Cu^{II}sGC	TEA, pH 7.4	1376	1504	1585	1641	this work
	Ni^{II}PPIX	TEA, pH 7.4	1378	1518	1592	1650, 1658	this work
	Ni^{II}PPIX	CTAB/base	1378	1519−1520	1592−1593	1657−1659	18
	Ni^{II}PPIX	CH_2Cl_2/CCl_4	1383	1520	1591	1656	43
	Ni^{II}Hb	P_i buffer	1378	1519	1592−1594	1657−1658	18
	Ni^{II}αHb	P_i buffer	NR	1517, 1520	1591	1653, 1657	19
	Ni^{II}MesoP	CTAB, pH 7	1381	1521	1605	1653, 1661	37
	Ni^{II}MP-11	CTAB, pH 7	1368, 1380	1519	1598	1651, 1660	37
	Ni^{II}cyt c	KCl, pH 1	1380	1519	1593	1658	27
	Cu^{II}PPIX	TEA, pH 7.4	1376	1503	1583	1641	this work
	Cu^{II}P	CS_2	1358		1562	1631	32
5	Ni^{II}Mb	P_i buffer	1368	1487−1488	1572−1573	1620	18
	Ni^{II}Hb	P_i buffer	1368	1485	1573−1574	1618−1620	18
	Cu^{II}PPIX	piperidine		1499	1578	1637	this work
6	Ni^{II}PPIX	piperidine	1364−1365	1476−1477	1564	1616−1617	18
	Ni^{II}PPIX	pyrrolidine	1364−1366	1475−1478	1563−1565	1616−1617	18
	Ni^{II}cyt c	P_i buffer, pH 7	1366	1479	1577, 1598		27

[a] NR = not reported.

suggested 4-coordination. Thus the data argue against histidine coordination in Cu^{II}sGC.

Porphyrin Planarity. Ni^{II}PPIX appears constrained to a planar conformation when bound to sGC. Several RR bands, notably the core vibrations ν_3, ν_2, ν_{37}, and ν_{10}, shift to higher frequency by 4−7 cm^{-1} when Ni^{II}PPIX binds to sGC (Figure 4 and Table 1). This effect is readily understood as a consequence of planarization of the porphyrin ring in the protein. Nickel porphyrins tend to undergo a ruffling distortion in order to accommodate the short Ni−N bond distance in the low-spin complex (*22*, *23*). Ruffling of the porphyrin ring lowers some of the vibrational frequencies, primarily as a result of kinematic effects (*24*). This phenomenon has been thoroughly studied in nickel octaethylporphyrin, because of the availability of crystalline polymorphs with both ruffled and planar structures (*25*, *26*). In solution there are a variety of ruffling modes (*18*, *19*, *24*), as evidenced in the breadth of the more sensitive RR bands, particularly ν_{10}. This phenomenon is observable in the solution RR spectrum of Ni^{II}PPIX (Figure 6). Alden et al. (*19*) have resolved the ν_{10} band of Ni^{II}PPIX in solution into two components by fitting the observed spectrum with two symmetrical peaks, and we obtain essentially the same result. The two components, at 1658 and 1652 cm^{-1}, can be assigned respectively to more and less planar structures. When Ni^{II}PPIX was bound to Hb, the lower-frequency component disappeared (*19*), consistent with discrimination of the heme-binding pocket against the ruffled structure. We see the same loss of the lower-frequency component in Ni^{II}sGC, consistent with selective binding of the planar conformer (Figure 4). Furthermore, in Ni^{II}sGC the ν_{10} band shifts to 1662 cm^{-1}. This observation contrasts with the behavior of Ni^{II}Hb, in which ν_{10} was observed at 1658 cm^{-1} (*19*), and with that of Ni^{II}cyt *c* at low pH (*27*), in which ν_{10} was observed at 1660 cm^{-1} (Table 6). We conclude from these differences that, within the heme-binding pocket of sGC, the porphyrin attains an even more planar structure than in Hb or cyt *c*.

Cu^{II}PPIX is bound by sGC without significant structural change. Because the $d_{x^2-y^2}$ orbital is singly occupied in Cu(II), the average Cu−N (1.99 Å) distance is longer than the average Ni−N (1.91 Å) distance and is readily accommodated by a planar porphyrin. Indeed the core of Cu^{II}PPIX is somewhat expanded relative to planar Ni^{II}PPIX, resulting in lowered core-size marker frequencies (Tables 4 and 5) (*28*). Unconstrained Cu(II) porphyrins are not ruffled; therefore, significant shifts are not observed when Cu^{II}PPIX binds in a planar conformation. Consistent with a lack of ruffling, the Cu^{II}PPIX ν_{10} band has only one component in solution. Binding to sGC results in small upshifts in Cu^{II}PPIX modes, but the effect is smaller than it is for Ni^{II}PPIX (Table 5), as expected if the porphyrin undergoes only minor structural perturbation on binding.

Vinyl Modes and the Heme Environment. Vibrational modes of the protoporphyrin vinyl substituents are potentially useful in elucidating the heme peripheral contacts in proteins. Typically, the vinyl modes of PPIX and its metal derivatives can be detected, albeit weakly, in Soret-resonant Raman spectra (*29*, *30*). The most distinctive of the vinyl features are the C=C stretches, at ∼1625 cm^{-1}. There are two of these stretches, usually about 10 cm^{-1} apart, corresponding to the two vinyl substituents, although sometimes one or the other is too weak to be observed. The frequencies are complex functions of the vinyl orientations and of coupling with porphyrin vibrations, and their predictive value is still under investigation.[2] Kalsbeck et al. (*31*) have presented evidence that rotation of the vinyl group into the porphyrin plane lowers the vinyl C=C frequency. For Cu^{II}PPIX, the two vinyl C=C bands are seen at 1634 and 1623 cm^{-1}, both in solution and in sGC (Figure 5 and Table 5). For Ni^{II}-PPIX, a single vinyl C=C band is seen, at 1635 cm^{-1} in solution and at 1631 cm^{-1} in sGC. The 4 cm^{-1} frequency lowering suggests some reorientation of one or both vinyl substituents toward the heme plane upon binding to the protein, possibly associated with the planarization of the porphyrin in sGC.

The most striking effect of the sGC environment is the substantial intensification of the vinyl RR bands for both

[2] Smulevich, G., and Marzocchi, M. Personal communication.

Cu^{II}PPIX and Ni^{II}PPIX. In solution these bands are difficult to discern, but they are quite prominent in the protein spectra. Clearly the vinyl bands are more strongly enhanced in the protein than they are in solution. Part of this effect may be due to the multiplicity of vinyl orientations in solution, which results in broadened bands (*31*). Spectral analysis by peak fitting indicated a narrowing of the vinyl bands in both Ni^{II}sGC and Cu^{II}sGC, although the substantial band overlap prevented quantitation of bandwidths in the fit. An alternative explanation for the intensification of the vinyl modes in Ni^{II}sGC and Cu^{II}sGC is that electric field effects in the protein contribute to the vinyl enhancements. This possibility is supported by the substantial shifts of the Soret absorptions when Cu^{II}PPIX and Ni^{II}PPIX bind to sGC. The shifts of the Soret absorptions to higher energy suggest the presence of negative charge or dipoles oriented with their negative ends toward the porphyrin. Such an environment would destabilize the π^* orbitals of the porphyrins, giving rise to an increase in the energy of the $\pi-\pi^*$ Soret absorption. Enhancement of the vinyl RR bands depends on the displacement of the electronic excited state along the vinyl vibrational coordinates, and this displacement might be increased by a protein-induced polarization of the electronic excited state. We note that independent evidence of negative polarity in the heme pocket of sGC has been advanced by Deinum et al. (*6*), who found an elevated CO frequency in the CO−heme adduct. It is possible that a negatively charged or dipolar group is positioned over the distal side of the heme pocket, between the bound CO and the vinyl groups, thereby accounting for both effects.

DISCUSSION

The results of prior studies on the mechanism of activation of sGC by NO have led us to postulate that the requirements for activation are 2-fold: (1) the presence of a porphyrin with the same peripheral substitution pattern as heme *b*; (2) the absence of an interaction with the proximal histidine ligand (*8*). To test this hypothesis, we have investigated the spectroscopic and kinetic effects of two four-coordinate metalloporphyrins on sGC. Ni^{II}PPIX and Cu^{II}PPIX were selected because they share the peripheral substitution pattern of the native heme *b*, but both exhibit a low affinity for axial ligands. Ni^{II}PPIX has been extensively characterized both free in solution and bound to a variety of heme proteins (*18, 19, 27, 29*). Furthermore, the vibrational frequencies of Ni^{II}PPIX are sensitive to the conformation of the porphyrin (*32*). Comparison of Ni(II)-substituted sGC to complexes of known structure was expected to provide valuable information about the heme binding site in sGC. Both Ni^{II}PPIX and Cu^{II}PPIX are unreactive toward oxygen; therefore, we anticipated that Ni(II)- and Cu(II)-substituted sGC would provide air stable protein samples in the active conformation.

Both Ni^{II}PPIX and Cu^{II}PPIX activated sGC significantly. The activity of neither Ni^{II}sGC nor Cu^{II}sGC was increased by the addition of NO. The apparent affinities of sGC for both porphyrins was very high; the activation constants were 24 and 17 nM for Ni^{II}PPIX and Cu^{II}PPIX, respectively. In this respect these metalloporphyrins are unique, as all other tight-binding metalloporphyrins inhibit sGC in the absence of NO. For example, FePPIX, MnPPIX, and ZnPPIX inhibited sGC with K_i values of 350, 9, and 50 nM, respectively (*9*). Dierks et al. (*8*) confirmed that Mn^{II}PPIX and Fe^{II}PPIX inhibited sGC activity and demonstrated that Co^{II}PPIX did so as well. Several free-base porphyrins are known that bind with high affinity and activate sGC. PPIX and mesoporphyrin activated sGC with a K_{act} of 8 nM for both porphyrins (*9*). The latter has the same substitution pattern as the former, but the vinyl groups are reduced to ethyl groups. Hematoporphyrin IX, in which the vinyl groups are replaced by hydroxyethyl groups, activates sGC, but the binding affinity is lowered by 1 order of magnitude (K_{act} of 76 nM) (*9*). Together these data seem to suggest that the presence of a metal ion results in inhibition of sGC rather than activation; however, our present observation that both Ni^{II}sGC and Cu^{II}sGC are activated is inconsistent with this interpretation.

Structural considerations provide an alternative explanation for porphyrin activation or inhibition. We have previously proposed that the presence of a metal−histidine bond results in inhibition and scission of the metal−ligand bond results in activation (*8*). Consistent with this interpretation, Fe^{II}sGC, Mn^{II}sGC, Co^{II}sGC, and Fe^{II}sGC(CO), all of which have been shown by spectroscopic methods to contain an intact metal−histidine bond, are not activated (*3*−*6*, *8*, *33*). In contrast, Fe^{II}sGC(NO) and Co^{II}sGC(NO), which are five coordinate with the axial histidine free, are fully activated (*8*). Free-base porphyrins are incapable of binding the axial ligand and are, by this analysis, expected to be activators. One other metalloporphyrin, Sn^{IV}PPIX, has been shown to activate sGC, but it does so with an activation constant of 4.9 μM, 2 orders of magnitude higher than other porphyrin activators of sGC (*11*). It was speculated that the low affinity of Sn^{IV}PPIX for sGC is a result of the coordination of the Sn atom by two water molecules, making the activating species SnPPIX-$(H_2O)_2^{2+}$. These considerations suggest the plausible explanation that Cu^{II}PPIX and Ni^{II}PPIX remain 4-coordinate when bound to sGC and are therefore activators because they do not bind the axial histidine ligand.

Spectroscopic characterization of Ni^{II}sGC and Cu^{II}sGC confirms 4-coordinate structures, thereby providing further support to the hypothesis that the absence of a metal−histidine bond is required for activation of sGC. Electronic absorption and RR spectral data are consistent with 4-coordination and inconsistent with 5-coordination, for Ni^{II}PPIX and Cu^{II}PPIX in sGC. Most notable in the electronic absorption spectra are the substantial shifts of the Soret absorption to higher energy on binding to sGC. The higher energy Soret absorptions are characteristic of Ni^{II}PPIX and Cu^{II}PPIX in 4-coordinate environments; the position of the bands below 400 nm are consistent with the porphyrins binding in a polar environment (*34*). RR spectra of Ni^{II}sGC are definitive for 4-coordination, as the ν_4 band does not shift upon binding to the protein. For Cu^{II}sGC, RR provide less conclusive evidence, but the high-frequency marker band positions are more similar to those of 4-coordinate Cu^{II}PPIX than to five coordinate Cu^{II}Mb or Cu^{II}PPIX(pip) (*35*, *36*), suggesting a 4-coordinate environment. Together these data clearly support a model where the activation of sGC is correlated with the absence of bond to the axial histidine ligand.

Despite similar coordination geometries, Ni^{II}PPIX and Cu^{II}PPIX differ in the extent to which they activate sGC; Ni^{II}PPIX is consistently a more effective activator than

Cu^{II}PPIX. One plausible explanation for this phenomenon is that even though the proximal histidine is not coordinated to either metal, its range of motion may be restricted by the electric field of the metal. The electric field is expected to be greater for Cu(II) than for Ni(II) because of the higher effective nuclear charge and the consequent contraction of the d_{z^2} orbital with its pair of electrons. Electrostatic effects may also account for the differences observed between the free-base PPIX and the four coordinate Ni^{II}PPIX and Cu^{II}PPIX. Activation of sGC by PPIX occurs with a low K_{act} (i.e. high affinity) and results in a higher maximal velocity (i.e. higher activity) than the four coordinate metalloporphyrins. However, the PPIX−sGC adduct cannot be isolated and the high initial activity of PPIX-activated sGC diminishes rapidly (*9*). Electrostatic attraction between the metal ion and the axial histidine might account for the lower lability as well as the lower activity for the four-coordinate metalloporphyrins.

Another possibility is that the global stability of the activated conformation of sGC may be related to the distortion of the porphyrin, as those tetrapyrroles that may undergo a transition from ruffled to planar structure upon binding sGC appear to be the most effective activators. Fe^{II}PPIX(NO) and Co^{II}PPIX(NO), the most effective activators of sGC, are likely to be ruffled in solution. Recent structural studies of related Fe(II)− and Co(II)−nitrosyl porphyrins reveal ruffling distortions of the porphyrin ring (*38*−*40*). Ni^{II}PPIX, which is ruffled in solution (*41*) and is also an effective sGC activator, becomes planar upon binding to sGC. The ν_{10} frequency of Ni^{II}sGC is higher than any previously observed, including that of the planar solution conformation and Ni^{II}Hb (*19*). These data suggest that sGC enforces a uniquely restricted planar conformation on the porphyrin. Cu^{II}PPIX is less ruffled in solution, and its binding to sGC produced weaker activation than Ni^{II}PPIX. We note that the crystal structure of free-base PPIX shows the porphyrin ring to be flat (*42*) but the solution structure is uncertain, and PPIX does not remain bound to sGC. It has been suggested elsewhere that nonplanar distortions of metalloporphyrins may provide a mechanism for proteins to control their porphyrin active sites (*19*, *27*, *37*). For sGC, the planarity of the metalloporphyrin cofactor may control the biological activity of the protein by altering the conformational equilibrium between activated and basal states. It is possible that the free energy of heme binding drives both the heme planarization and the conformational shift from basal to active state. Furthermore, it is plausible that the stability of the activated state of sGC in the presence of a tetrapyrrole correlates with a preference for a ruffled conformation in solution.

There appear to be three broad categories of sGC-activating tetrapyrroles: (1) planar free-base porphyrins; (2) 4-coordinate metalloporphyrins; (3) 5-coordinate nitrosyl−metalloporphyrins. For the first category, the free-base porphyrins, the key structural feature leading to activation is the peripheral substitution pattern. Only PPIX, and the very closely related mesoporphyrin and hematoporphyrin, are activators of sGC (*9*). The observation of substantial enhancement of the vinyl modes of the porphyrin periphery in Ni^{II}sGC suggests that the protein may restrict the conformational mobility of the vinyl groups, possibly by providing specific hydrophobic binding pockets. For the 4-coordinate metalloporphyrins, a preference for a ruffled solution conformation, as is observed in Ni^{II}PPIX, correlates with more efficient activation of the enzyme. The five coordinate nitrosyl−metalloporphyrins Fe^{II}PPIX(NO) and Co^{II}PPIX(NO) are the most potent activating tetrapyrroles known (*8*). In addition to likely favoring a ruffled conformation in solution, these metalloporphyrins possess the appended NO ligand, which may make important electrostatic interactions in the distal pocket that stabilize the activated conformation. All these considerations suggest that the binding of the tetrapyrrole is more constrained in the active conformation than in the basal conformation, and the shape and electrostatic character of the tetrapyrrole are important contributors to the stability of activated sGC.

REFERENCES

1. Hobbs, A. J. (1997) *Trends Pharmacol. Sci. 18*, 484−491.
2. Wolin, M. S., Wood, K. S., and Ignarro, L. J. (1982) *J. Biol. Chem. 257*, 13312−13320.
3. Yu, A. E., Hu, S., Spiro, T. G., and Burstyn, J. N. (1994) *J. Am. Chem. Soc. 116*, 4117−4118.
4. Stone, J. R., and Marletta, M. A. (1994) *Biochemistry 33*, 5636−5640.
5. Burstyn, J. N., Yu, A. E., Dierks, E. A., Hawkins, B. K., and Dawson, J. H. (1995) *Biochemistry 34*, 5896−5903.
6. Deinum, G., Stone, J. R., Babcock, G. T., and Marletta, M. A. (1996) *Biochemistry 35*, 1540−1547.
7. Stone, J. R., Sands, R. H., Dunham, W. R., and Marletta, M. A. (1995) *Biochem. Biophys. Res. Commun. 207*, 572−577.
8. Dierks, E. A., Hu, S., Vogel, K. M., Yu, A. E., Spiro, T. G., and Burstyn, J. N. (1997) *J. Am. Chem. Soc. 119*, 7316−7323.
9. Ignarro, L. J., Ballot, B., and Wood, K. S. (1984) *J. Biol. Chem. 259*, 6201−6207.
10. Ignarro, L. J., Wood, K. S., and Wolin, M. S. (1982) *Proc. Natl. Acad. Sci. U.S.A. 79*, 2870−2873.
11. Serfass, L., and Burstyn, J. N. (1998) *Arch. Biochem. Biophys. 359*, 8−16.
12. Serfass, L., Carr, H. S., Aschenbrenner, L. M., and Burstyn, J. N. (2001) *Arch. Biochem. Biophys. 387*, 47−56.
13. Kim, T. D., and Burstyn, J. N. (1994) *J. Biol. Chem. 269*, 15540−15545.
14. Cleland, W. W. (1979) *Methods Enzymol. 63*, 103−138.
15. Foerster, J., Harteneck, C., Malkewitz, J., Schultz, G., and Koesling, D. (1996) *Eur. J. Biochem. 240*, 380−386.
16. Dong, S., Padmakumar, R., Banerjee, R., and Spiro, T. G. (1999) *J. Am. Chem. Soc. 121*, 7063−7070.
17. Zhao, X., Chen, R., Tengroth, C., and Spiro, T. G. (1999) *Appl. Spectrosc. 53*, 1200−1205.
18. Shelnutt, J. A., Alston, K., Ho, J.-Y., Yu, N.-T., Yamamoto, T., and Rifkind, J. M. (1986) *Biochemistry 25*, 620−627.
19. Alden, R. G., Ondrias, M. R., and Shelnutt, J. A. (1990) *J. Am. Chem. Soc. 112*, 691−697.
20. Spiro, T. G., and Li, X.-Y. (1988) in *Biological Applications of Raman Spectroscopy* (Spiro, T. G., Ed.) pp 1−38, Wiley, New York.
21. Kim, D., and Spiro, T. G. (1986) *J. Am. Chem. Soc. 108*, 2099−2100.
22. Hoard, J. L. (1971) *Science 174*, 1295−1302.
23. Kozlowski, P. M., Rush, T. S. I., Jarzecki, A. A., Zgierski, M. Z., Chase, B., Piffat, C., Ye, B.-H., Li, X.-Y., Pulay, P., and Spiro, T. G. (1999) *J. Phys. Chem. A 103*, 1357−1366.
24. Prendergast, K., and Spiro, T. G. (1992) *J. Am. Chem. Soc. 114*, 3793−3801.
25. Czernuszewicz, R. S., Li, X.-Y., and Spiro, T. G. (1989) *J. Am. Chem. Soc. 111*, 7024−7031.
26. Jentzen, W., Unger, E., Karvounis, G., Shelnutt, J. A., Dreybrodt, W., and Schweitzer-Stenner, R. (1996) *J. Phys. Chem. 100*, 14184−14191.
27. Ma, J.-G., Laberge, M., Song, X.-Z., Jentzen, W., Jia, S.-L., Zhang, J., Vanderkooi, J. M., and Shelnutt, J. A. (1998) *Biochemistry 37*, 5118−5128.
28. Parthasarathi, N., Hansen, C., Yamaguchi, S., and Spiro, T. G. (1987) *J. Am. Chem. Soc. 109*, 3865−3871.

29. Choi, S., Spiro, T. G., Langry, K. C., and Smith, K. M. (1982) *J. Am. Chem. Soc. 104*, 4337−4344.
30. Smulevich, G., Hu, S., Rodgers, K. R., Goodin, D. B., Smith, K. M., and Spiro, T. G. (1996) *Biospectroscopy 2*, 365−376.
31. Kalsbeck, W. A., Ghosh, A., Pandey, R. K., Smith, K. M., and Bocian, D. F. (1995) *J. Am. Chem. Soc. 117*, 10959−10968.
32. Jentzen, W., Turowska-Tyrk, I., Scheidt, W. R., and Shelnutt, J. A. (1996) *Inorg. Chem. 35*, 3559−3567.
33. Vogel, K. M., Hu, S., Spiro, T. G., Dierks, E. A., Yu, A. E., and Burstyn, J. N. (1999) *J. Biol. Inorg. Chem. 4*, 804−813.
34. Kolling, O. W. (1989) *J. Phys. Chem. 93*, 3436−3439.
35. Alston, K., and Storm, C. B. (1979) *Biochemistry 18*, 4292−4300.
36. Manoharan, P. T., Alston, K., and Rifkind, J. M. (1986) *J. Am. Chem. Soc. 108*, 7095−7100.
37. Ma, J.-G., Vanderkooi, J. M., Zhang, J., Jia, S.-L., and John A. S. (1999) *Biochemistry 38*, 2787−2795.
38. Richter-Addo, G. B., Hodge, S. J., Yi, G.-B., Khan, M. A., Ma, T., Caemelbecke, E. V., Guo, N., and Kadish, K. M. (1996) *Inorg. Chem. 35*, 6530−6538.
39. Ellison, M. K., and Scheidt, W. R. (1997) *J. Am. Chem. Soc. 119*, 7404−7405.
40. Scheidt, W. R., Duval, H. F., Neal, T. J., and Ellison, M. K. (2000) *J. Am. Chem. Soc. 122*, 4651−4659.
41. Jentzen, W., Unger, E., Song, X.-Z., Jia, S.-L., Turowska-Tyrk, H., Schweizer-Stenner, R., Dreybrodt, W., Scheidt, W. R., and Shelnutt, J. A. (1997) *J. Phys. Chem. A 101*, 5789−5798.
42. Caughey, W. S., and Ibers, J. A. (1977) *J. Am. Chem. Soc. 99*, 6639−6645.
43. Lee, H., Kitagawa, T., Abe, M., Pandey, R. K., Leung, H.-K., and Smith, K. M. (1986) *J. Mol. Struct. 146*, 329−347.

BI010777K